DESIGN AND PARAMETER IDENTIFICATION BY LABORATORY EXPERIMENTS OF A PROTOTYPE MODULAR ROBOTIC ARM FOR ORBITING SPACECRAFT APPLICATIONS

Josep Virgili-Llop, Jerry V. Drew II, Marcello Romano

Spacecraft Robotics Laboratory
Naval Postgraduate School
Monterey CA USA

ABSTRACT

This paper describes the design and the parameter identification procedure of a modular spacecraft robotic arm developed for an air-bearing table experimental test bed. When combined with the necessary ancillary equipment (base-spacecraft, target, and end-effector), the system provides an experimental setup where control approaches and whole mission scenarios (e.g. de-tumbling, servicing, and debris removal) can be validated and demonstrated. The originality of this newly developed manipulator consists in its modularity. Each manipulator link contains its own power system, communications, harmonic drive servomotor with integrated encoder, controller, torque sensor, and computing platform. The link bodies themselves are produced using additive manufacturing, allowing quick and inexpensive generation of differently sized links (with different mass and inertia properties). The links are easily rearranged to meet different mission requirements or experimental objectives. The experimentation in this uses a four-link serial manipulator with four rotational degrees-of-freedom. Each link has a length of $\sim$40 cm and a mass of $\sim$3 kg. The manipulator attaches to a ˜10 kg Floating Spacecraft Simulator that floats via air bearings over a 4-by-4 meter granite monolith to simulate, in two dimensions, the reduced gravity and quasi-frictionless environment of space. As the system operates in a planar environment, its movement is restricted to three degrees-of-freedom (two translational and one rotational).

Index Terms— space robotics, parameter identification, experimental

1. INTRODUCTION

A spacecraft equipped with a robotic arm can be called upon to fulfill a wide range of missions (e.g. de-tumbling, servicing, and debris removal). Although spacecraft robotic arms have been flown in the past, they have most often been used in conjunction with large spacecraft (e.g. the International Space Station [1, 2, 3]). When compared to its base-spacecraft, a manipulator with a relatively small mass and inertia exhibits low dynamic coupling between the manipulator motion and the base-spacecraft reaction. With the trend towards smaller, more capable satellites and the desire to reduce the mass penalty during launch, future missions may require one or more manipulators mounted on smaller spacecraft—a situation that generates significant dynamic coupling and presents a considerable control challenge (as demonstrated during the ETS-VII [4] and the Orbital Express [5, 6] missions). To advance space robotics, conduct mission rehearsals, validate hardware components, or develop novel control schemes, experimental validation within a dynamically relevant environment is critical.

Unlike terrestrial fixed-base manipulators, space-based manipulators are attached to a floating base that is free to react to the manipulator motion. This dynamic coupling, combined with non-linear manipulator dynamics, results in a complex dynamical system that is difficult to control. When other effects such as elasticity in the links and joints, joint friction, actuator dead bands, and other non-linearities are taken into consideration, the system becomes very difficult to simulate in a virtual environment, and experimental validation of control techniques may be required. Although replicating the frictionless, reduced-gravity, and variable-lighting aspects of the space environment are difficult to achieve on the ground, several types of experimental facilities exist which attempt to solve these challenges.

There are two basic families of spacecraft simulators: kinematic and dynamic simulators. Kinematic simulators are common for rendezvous and proximity operations and are very useful for kinematics related research (e.g. path planning), but they rely on computer simulations to generate the dynamics and are therefore not particularly well suited for dynamics research [7].

Dynamic simulators [8] based on air-bearing tables or flat floors [9, 10, 11, 12], neutral buoyancy pools [13, 7], free-fall chambers, and suspension systems have long been in use for space robotics research. These type of simulators recreate the quasi-frictionless and reduced gravity environment, being able to recreate the dynamic behavior of spacecraft-manipulator system. Each type of dynamic simulator has advantages and disadvantages, but due to the its flexibility, rela-

tively low cost, ease of use, and the short turn-around time between experiments, the air-bearing systems are the most common.

This paper presents the work done at the Naval Postgraduate School (NPS) to establish a dynamic simulator test bed on an air-bearing table, where advanced space robotics control techniques and full mission scenarios with multiple vehicles can be tested and validated prior to flight. First, a general overview of the Floating Spacecraft Simulator (NPS-FSS) test bed and its capabilities is provided for completeness. An overview of the modular manipulator hardware and software follows. Since the manipulator can be arranged in a number of different configurations, a method to identify the manipulator parameters (mainly mass, inertia, and the Denavit-Hartenberg or DH parameters) is then presented. Finally, a brief workspace and manipulability analysis of the complete system is provided.

2. FLOATING SPACECRAFT SIMULATOR TESTBED OVERVIEW

The robotic manipulator is attached to a Floating Spacecraft Simulators (FSS) that floats via air-pads over a 4-by-4 meter polished granite monolith surface recreating a reduced gravity and a quasi-friction-less motion in two translational and one rotational degrees-of-freedom (planar motion) [14, 15, 16, 17, 18, 19, 20, 21, 22, 23]. Figure 1 shows two FSS, one with the modular robotic manipulator, over the granite surface.

The $\sim$10 kg FSS have eight cold-gas thrusters which provide autonomous motion capability to the vehicles. An on-board tank of compressed air (propellant), a power system and on-board computer give them full autonomy. All the required processing (sensor readings, communications, navigation, guidance and control, and actuator commanding) is handled on-board in real-time.

An RTAI patched Server Edition Ubuntu 14.04 operating system is used to provide multi-rate real-time execution capabilities to the FSS. The guidance, navigation and control algorithms are developed in MATLAB/Simulink, compiled in a development machine, and later transferred to the FSS internal memory prior to execution.

Navigation data is provided by an overhead motion capture system (VICON), providing position and attitude, augmented by an on-board one-axis Fiber Optics Gyroscope (FOG). Communication between multiple FSS, the VICON workstation and other PC (used for telemetry monitoring and software upload) is achieved by sending and receiving data packets using the TCP/UDP protocol over an ad-hoc Wi-Fi network.

3. MODULAR MANIPULATOR HARDWARE DESCRIPTION

The manipulator has been designed to be as modular as possible, making it easy to reconfigure and upgrade. Each link of the manipulator includes all of the hardware required to operate independently from every other link. Each link has its own power subsystem (battery and power regulators), joint actuator and sensor, air bearing with tubing and connectors, and a Wi-Fi-connected micro-controller. Multiple links are connected together to obtain a multi-degree-of-freedom manipulator. The compressed air for the air bearings is provided by the main tank on the FSS, and the feed tubing is daisy-chained from link to link. A general view of this modular link is shown in Fig. 2 simulating a capture mission scenario.

When connected to the FSS, which acts as the base-spacecraft, a fully functional spacecraft-manipulator system is obtained. Each link uses its Wi-Fi connection to transmit telemetry to and receive commands from the base-spacecraft using UDP/TCP datagrams at a 5 Hz rate. The link micro-controller is only used as a relay, and all the Guidance Navigation and Control algorithms are executed on the base-spacecraft.

Each link has its own revolute joint actuated by a 1.8 Nm maximum torque harmonic servomotor. The actuator, which includes an encoder, is controlled via a driver that allows command in current, position, or velocity modes. The driver provides telemetry about the actuator angular position, velocity, and current consumed (proportional to the torque). Additionally, an analog 2.1 Nm torque sensor is mounted alongside the servo actuator. A load cell amplifier with a 24-bit analog-to-digital converter obtains the torque readings. The commanding of the driver and processing of the torque measurements is done through an Arduino-based stack. An Arduino Due board provides the main processing power. The communication with the driver is enabled by an RS-232 expansion shield. A Wi-Fi shield completes the stack, providing connectivity to the FSS base spacecraft. All of the link equipment is powered through a 14.4 V, 89 Wh lithium-ion battery. A DC-DC converter provides the 24 V required by the driver and a Low Dropout Regulator with clip-in heat sink provides the 5V power supply to the Arduino stack. An annotated view of one of the links is provided in Fig. 3.

All of the link equipment is housed in a custom-made, polycarbonate enclosure. The additive manufacturing process allows the structure to be quickly modified to suit particular mission needs or to accommodate upgraded components. Each link has a mass of $\sim$3 kg and is approximately 39 cm long from joint to joint. Due to geometry constraints, the joint rotations are limited to $\pm$90 degrees. The link's weight and dimensions are other areas that could be improved for future design iterations. When four links are connected, the total manipulator mass is similar to the FSS base spacecraft mass. The inertia of the manipulator, when fully extended,

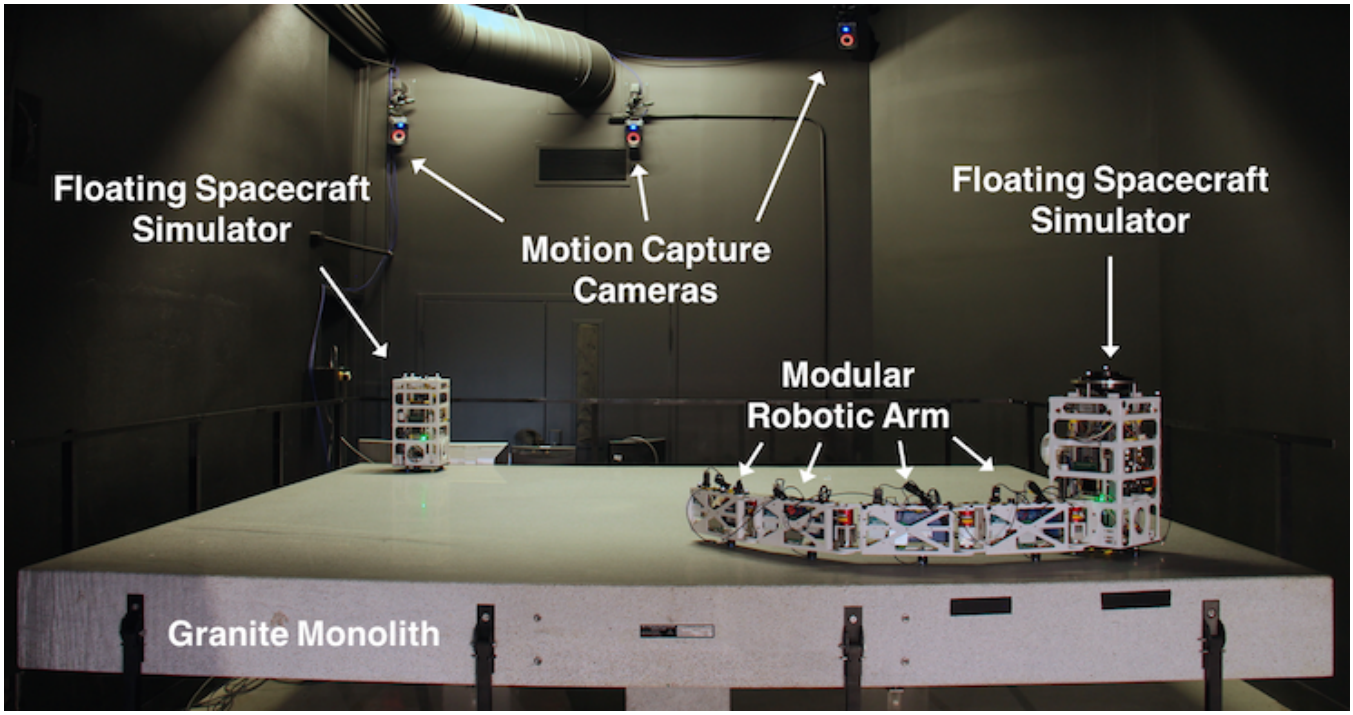

Fig. 1: Floating Spacecraft Simulator and the modular robotic arm on top of the 4-by-4 meter granite surface.

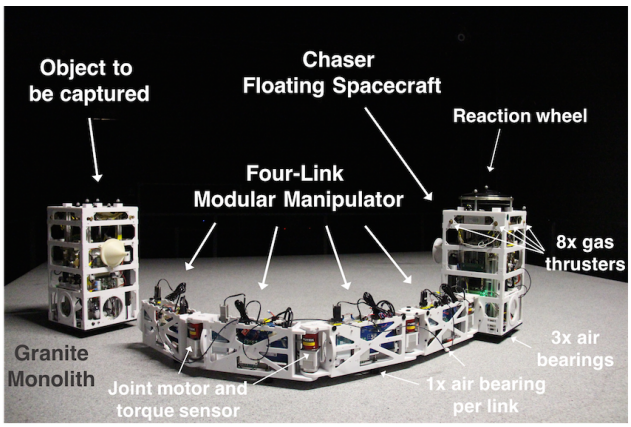

Fig. 2: Schematic representation of a Floating Spacecraft Simulator with the modular manipulator in a capture mission scenario.

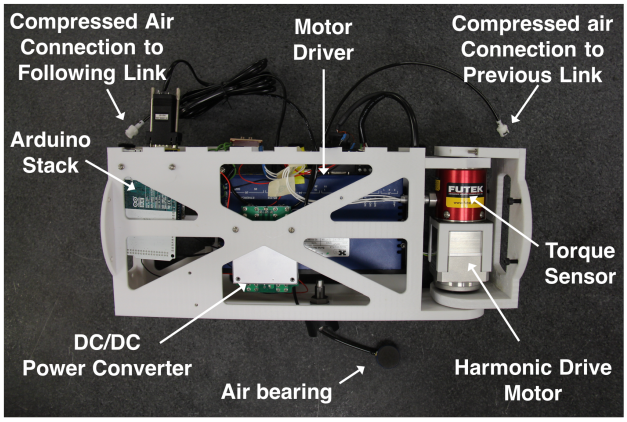

Fig. 3: Annotated view of on link of the modular manipulator.

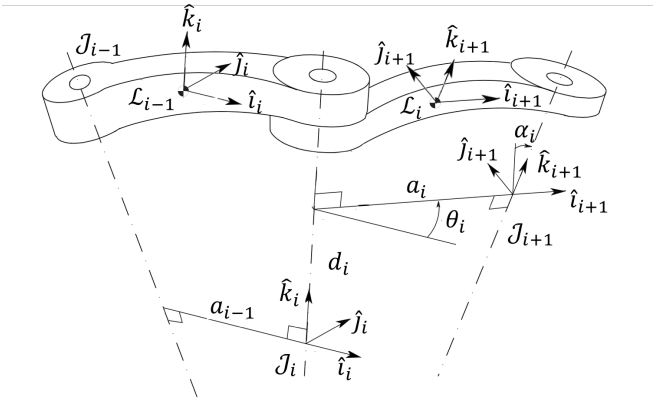

Fig. 4: Denavit-Hartenberg parameters (adapted from [25]).

greatly surpasses the FSS inertia. This large mass and inertia causes a strong dynamic coupling between the manipulator and the base spacecraft that may be detrimental to some applications. Additionally, the currently-used Arduino Wi-Fi shield has been discontinued and will eventually require an upgrade when a replacement is required.

As the spacercraft-manipualtor system operates on an air-bearing table, it is only able to recreate planar dynamics (two translational and one rotational degrees-of-freedom). Three links would then have been enough to achieve any desired state of the end-effector. The forth link provides kinematic redundancy to the system, allowing investigation of control approaches for redundant manipulators (e.g. a zero reaction maneuver [24] which uses the redundant degree-of-freedom to eliminate any rotational base-reaction).

4. PARAMETER IDENTIFICATION

Once the manipulator has been assembled, a calibration process is required to determine certain kinematic and dynamic parameters. The kinematics relate the base spacecraft state q_0 and joint states q_m with the end-effector state x_{EE}. The kinematic relationship between joints can be expressed using the Denavit-Harteneberg (DH) convention shown in Fig. 4 [25, 26].

In the DH convention, there are four different parameters that univocally describe the relationship between the $\mathcal{J}_{i+1}$ and $\mathcal{J}_i$ joint frames. These parameters are shown in Fig. 4 and their geometric definition is provided in Table 1. Note that these parameters need to be defined for each pair of connected joints.

The current manipulator design and experimental set-up only allows for planar motion and revolute joint types. It is then clear that $d = \alpha = 0$, leaving only two DH parameters left for the calibration. The θ angle is the revolute joint variable and thus it is not traditionally considered as a parameter but offsets between the commanded and true revolute joint variables may exist and thus an offset θ_{0i} parameter will be included.

In addition, if a base-spacecraft frame $\mathcal{B}_0$ is defined there are three more parameters, location $x_{\mathcal{BJ}_1}, y_{\mathcal{BJ}_1}$ and orientation $\theta_{\mathcal{BJ}_1}$ of the first joint with respect to the base, that need to be defined. The kinematic relationship can then be expressed as follows.

$$x_{EE} = k\left(\theta, \theta_0, a, x_{\mathcal{BJ}_1}, y_{\mathcal{BJ}_1}, \theta_{\mathcal{BJ}_1}\right) \tag{1}$$

The dynamic parameters are simply the mass of each link m_i, the location of the link's center-of-mass and its inertia I_i in the local link coordinates $\mathcal{L}_i$. As the link frame origin is attached to the link center-of-mass the vector from the center-of-mass to the next joint b_i is also a dynamic parameter.

4.1. Kinematic Calibration

An iterative batch least square method is used to perform the kinematic calibration. In this process, an initial guess of the kinematic parameters will be iteratively refined to produce a set of parameters that minimize the error of the end-effector state x_{EE} when comparing the kinematic model with respect to multiple experimental observations.

For each link there are two different parameters θ_{0i}, a_i that need to be estimated and three additional ones for the base-spacecraft $x_{\mathcal{BJ}_1}, y_{\mathcal{BJ}_1}, \theta_{\mathcal{BJ}_1}$. Note that the angular offset of the first joint θ_{01} and the orientation offset from the base to the first joint $\theta_{\mathcal{BJ}_1}$ represent the same magnitude and thus it will be assumed that $\theta_{01} = 0$. For an n link planar manipulator there will be $2n + 2$ parameters to estimate. These parameters can then be arranged in the ξ_k $2n + 2$ one-dimensional vector. The state of the end-effector x_{EE} consists of three different states (position and orientation).

To determine these parameters, multiple experimental observations of the end-effector state x_{EE} are conducted for a wide range of manipulator configurations. The joint variables θ_i on the experimental observations are also recorded.

If s denotes the number of experimental observation, these can be arranged in a $3s$ one-dimensional vector as $\hat{x}_{EE}$. Using the current kinematic parameter estimates (or the initial guess in the first iteration), the end-effector state, according to the kinematic model, can be computed for the different experimental configurations and also arranged as a $3s$ one-dimensional vector $\tilde{x}_{EE}$. The difference between the experimental observations and the states derived from the kinematic model is denoted by Δx_{EE} and can be expressed as in Eq. (2).

$$\Delta x_{EE} = \hat{x}_{EE} - \tilde{x}_{EE} \tag{2}$$

By linearizing the kinematics model, a batch least square solution on the parameters ξ differences can be obtained by iteratively using Eq. (4). The Φ_k $3s \times 2n + 2$ matrix is the Jacobian of the kinematic function (shown in Eq. (1)) at the different observation configurations.

Table 1: Denavit-Hartenberg parameters and their geometric definition.

DH parameter	Geometric definition
$d_{i,i+1}$	Distance between the $\mathcal{J}_i$ and $\mathcal{J}_{i+1}$ origins along the $\hat{k}_i$ axis. It is also the prismatic joint variable.
$\theta_{i,i+1}$	Rotation from $\hat{i}_i$ to $\hat{i}_{i+1}$ along $\hat{k}_i$. It is also the revolute joint variable.
$\alpha_{i,i+1}$	Rotation from $\hat{k}_i$ to $\hat{k}_{i+1}$ along $\hat{j}_{i+1}$.
$a_{i,i+1}$	Distance along the common normal between $\hat{k}_i$ and $\hat{k}_{i+1}$

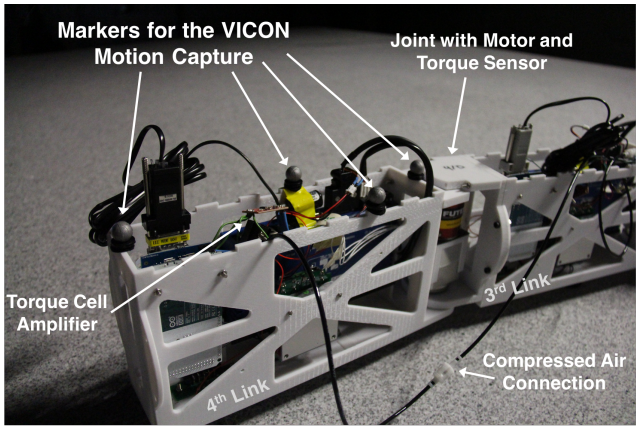

Fig. 5: Markers on the end-link used for the kinematic calibration.

$$\Delta x_{EE} = \Phi_k \Delta \xi_k \tag{3}$$

$$\Delta \xi_k = \left(\Phi_k^T \Phi_k\right)^{-1} \Phi_k^T \Delta x_{EE} \tag{4}$$

$$\Phi_k = \begin{bmatrix} \frac{\partial k}{\partial \theta_0}_1 & \frac{\partial k}{\partial a}_1 & \frac{\partial k}{\partial x_{\mathcal{B}\mathcal{J}_1}}_1 & \frac{\partial k}{\partial y_{\mathcal{B}\mathcal{J}_1}}_1 & \frac{\partial k}{\partial \theta_{\mathcal{B}\mathcal{J}_1}}_1 \\ \vdots & \vdots & \vdots & \vdots & \vdots \\ \frac{\partial k}{\partial \theta_0}_s & \frac{\partial k}{\partial a}_s & \frac{\partial k}{\partial x_{\mathcal{B}\mathcal{J}_1}}_s & \frac{\partial k}{\partial y_{\mathcal{B}\mathcal{J}_1}}_s & \frac{\partial k}{\partial \theta_{\mathcal{B}\mathcal{J}_1}}_s \end{bmatrix} \tag{5}$$

The results of Eq. (4) are used to update the kinematic parameter vector ξ_k (initially set with an initial guess) and the procedure is repeated (using the same experimental results) until the variations on the parameters is below a certain threshold $\Delta\xi_k < \epsilon$.

Figure 5 shows the kinematic calibration experimental set-up. The VICON motion capture system is used to obtain the end-effector x_{EE} and base-spacecraft states, while the telemetry of the manipulator links provide the joint angles for the different observations. As all the links are geometrically identical, it is assumed that the a parameter is the same for all the links except the last one (which is missing a subsequent joint and thus is slightly shorter).

Table 2: Manipulator kinematic parameters.

	Link 1	Link 2	Link 3	Link 4
a_i [m]	0.3825	0.3825	0.3825	0.3351
θ_{0_i} [degrees]	0	5.801	-3.402	-1.391

Table 3: Base to first joint kinematic parameters.

Parameters	Value
$x_{\mathcal{B}\mathcal{J}_1}$[m]	0.2058
$y_{\mathcal{B}\mathcal{J}_1}$[m]	0.0155
$\theta_{\mathcal{B}\mathcal{J}_1}$ [degrees]	18.211

The results of the kinematic calibration, using 13 measurements, are shown in Table 2 and 3. The standard deviation of the residuals is 0.015 m and 0.683 deg for the position and orientation of the end-effector respectively.

4.2. Dynamic Calibration

The dynamic calibration is performed by taking advantage of the non-holonomic constraint imposed by the base-spacecraft. For a floating-base case with no external forces, the final base-spacecraft state after a manipulator maneuver is completed is dependent on the manipulator path followed in joint space $q_m(t)$ and on the dynamic properties of the manipulator links.

If it is assumed that all the other system properties are known (including the manipulator kinematic parameters and the mass and inertia parameters of the base-spacecraft), the final state of the base-spacecraft can be written as in Eq. (6) with $d()$ being the dynamics function.

$$q_{0_f} = d\left(b, m, I, \theta\left(t\right)\right) \tag{6}$$

The number of parameters to determine are $3n$ and a similar batch least square procedure can then be performed. Let $\hat{q}_{0_f}$ and $\tilde{q}_{0_f}$ denote the observed and predicted (using the dynamic function) base-spacecraft states respectively.

$$\Delta q_{0_f} = \hat{q}_{0_f} - \tilde{q}_{0_f} \tag{7}$$

$$\Delta q_{0_f} = \Phi_d \Delta \xi_d \tag{8}$$

Table 4: Manipulator dynamic parameters.

	Link 1	Link 2	Link 3	Link 4
m_i [kg]	2.88	2.88	2.88	2.88
b_i [m]	0.191	0.191	0.191	0.168
I_i [kg m^2]	0.034	0.034	0.034	0.034

$$\Delta\xi_d = \left(\Phi_d^T \Phi_d\right)^{-1} \Phi_d^T \Delta q_{0_f} \tag{9}$$

$$\Phi_d = \begin{bmatrix} \frac{\partial d}{\partial b}_1 & \frac{\partial d}{\partial m}_1 & \frac{\partial d}{\partial I}_1 \\ \vdots & \vdots & \vdots \\ \frac{\partial d}{\partial b}_s & \frac{\partial d}{\partial m}_s & \frac{\partial d}{\partial I}_s \end{bmatrix} \tag{10}$$

The same experimental set-up described in section 4.1 is used for the dynamic calibration. To simplify the calibration, each measurement, which corresponds to a unique maneuver, is done only varying one joint angle. If this is the case, the path is then simply reduced to the initial and final joint angles (simplifying the experimental procedure).

The masses of the links can be measured with a scale, and it will be assumed that all links have the same mass. Although the reaction of the base is considerable (specially when the first joint moves) the dynamic calibration procedure is very sensitive to measurement uncertainty (mainly uncertainty on the state of the base-spacecraft). Although every precaution has been taken to obtain accurate data, the link's center-of-mass location is poorly observable and thus the calibration procedure doe not yield accurate results. Therefore, it has been assumed that the link's center-of-mass lies in the geometric center of each link.

To simplify the dynamic calibration even further, it is assumed that all links have the same inertia. All these assumptions reduce to the number of parameters to be estimated by the dynamic calibration to only one, the inertia of the links I.

The results of the dynamic calibration, using 8 unique maneuvers, are shown in Table 4. The standard deviation of the residuals for the base-spacecraft orientation after a maneuver is 1.54 degrees.

5. WORKSPACE AND MANIPULABILITY ANALYSIS

The workspace is defined as the reachable volume by an end-effector. The primary workspace is where the end-effector can reach regardless of its orientation (reachable workspace) [25].

The case of a flying spacecraft that remains fixed in inertial space (counteracting the manipulator coupling) is equivalent to a manipulator with a fixed-based, and its workspace is then limited by the manipulator geometry and its joint limits. This workspace is referred to as the fixed vehicle workspace and can be obtained using analytical or numerical methods

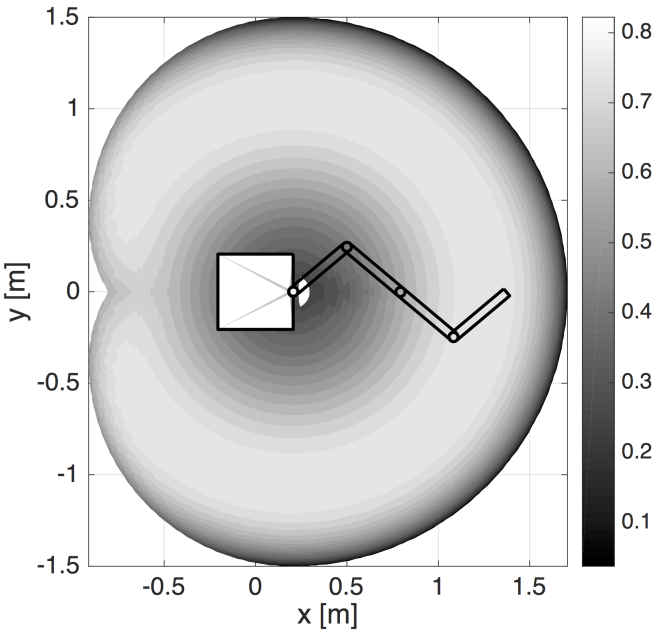

Fig. 6: Fixed vehicle workspace and kinematic manipulability measure.

[27, 28, 29, 30, 31]. The fixed vehicle workspace of the designed modular manipulator is shown in Fig. (6).

Due to the non-holonomic constraint imposed by the base-spacecraft, the workspace for a floating case (where the base freely reacts to the manipulator motion) is more difficult to define. In the maximum reachable workspace, the path of the manipulator is not specified, and it can be assumed that the spacecraft is able to reorient itself through manipulator cyclic motion. This workspace is then a sphere centered around the system's center-of-mass and with the radius defined by Eq. (13), where g_i is the distance from the link's center-of-mass to its previous joint. The R radius is also the total length of the equivalent virtual manipulator [32, 33]). For the four-link presented manipulator $R = 1.3$ m,

$$b_i^{VM} = b_i \frac{\sum_{k=0}^{i} m_k}{m_{\text{tot}}} \tag{11}$$

$$g_i^{VM} = g_i \frac{\sum_{k=0}^{i-1} m_k}{m_{\text{tot}}} \tag{12}$$

$$R = \sum_{i=0}^{n} (b_i^{VM} + g_i^{VM}) \tag{13}$$

A more useful workspace measure is the straight-path workspace, which is defined as the volume that can be reached if the point of interest (e.g. end-effector) is moved in a straight line from the starting configuration. This volume is obviously continuous and its boundary can be numerically obtained by subsequently moving the manipulator until it is no longer possible to maintain a straight line motion. Geometric and

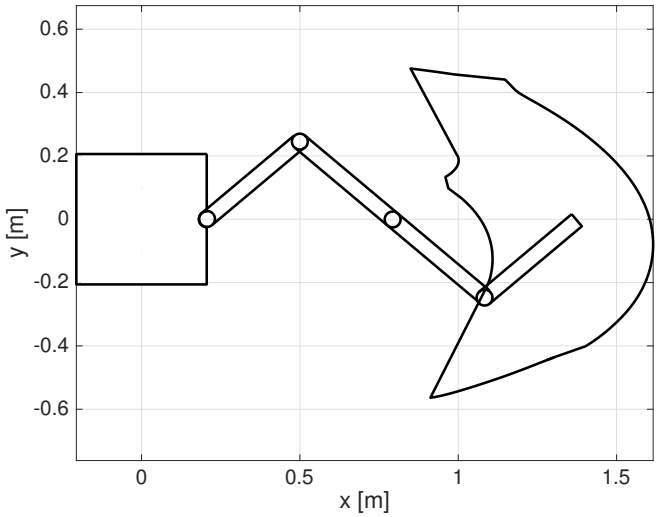

Fig. 7: Floating straight-path workspace.

joint limits can be included when obtaining this workspace. An example of this workspace is provided in Fig. 7. To produce Fig. 7 the joint limits are considered when three of the four joints have reached their limits. The kinematic redundancy is thus exploited to avoid driving the joints towards their limits As expected, due to the low mass and inertia of the base-spacecraft when compared to the manipulator ones, this workspace is much more limited than its fixed-base counterpart.

The kinematic manipulability ellipsoid provides a quantitative measure of the ability to move a manipulator point (usually the end-effector) in a particular direction and to obtain the velocity transmission ratio from joint space to operational space along that direction. These ellipsoids are a tool to seek optimal manipulator configurations to perform a task in a certain direction. An example of fixed-base and floating base kinematic manipulability ellipsoids is provided in Fig. 8. As expected the fixed-base ellipsoid is much larger than its floating base counterpart. The area of the ellipsoid is known as the kinematic manipulability measure, and for the fixed-base case, this is shown in Fig. 6.

6. CONCLUSIONS

A four-link modular robotic manipulator has been designed and built to operate on a air-bearing table test setup. When connected to a base-spacecraft the system is able to recreate the planar dynamics of a spacecraft-manipulator system. The modularity of the links allows rapid rearrangement and adaptation of the system to the type of test to be conducted. Four links have been built as it provides one extra degree-of-freedom, providing kinematic redundancy and allowing the investigation of control approaches for redundant manipulators.

7. REFERENCES

[1] M.F. Stieber, C.P. Trudel, and D.G. Hunter, "Robotic systems for the international space station," in *Robotics and Automation, 1997. Proceedings., 1997 IEEE International Conference on*, Apr 1997, vol. 4, pp. 3068–3073 vol.4.

[2] Naoki Sato and Yasufumi Wakabayashi, "Emrms design features and topics from testing.," in *6th International symposium on artificial intelligence, robotics and automation in space (iSAIRAS). Quebec.*, 2001.

[3] Elliott Coleshill, Layi Oshinowo, Richard Rembala, Bardia Bina, Daniel Rey, and Shelley Sindelar, "Dextre: Improving maintenance operations on the international space station," *Acta Astronautica*, vol. 64, no. 9–10, pp. 869 – 874, 2009.

[4] M. Oda, "Experiences and lessons learned from the etsvii robot satellite," in *Robotics and Automation, 2000. Proceedings. ICRA '00. IEEE International Conference on*, 2000, vol. 1, pp. 914–919 vol.1.

[5] James Shoemaker and Melissa Wright, "Orbital express space operations architecture program," in *Defense and Security*. International Society for Optics and Photonics, 2004, pp. 57–65.

[6] Andrew Ogilvie, Justin Allport, Michael Hannah, and John Lymer, "Autonomous satellite servicing using the orbital express demonstration manipulator system," in *Proc. of the 9th International Symposium on Artificial Intelligence, Robotics and Automation in Space (iSAIRAS'08)*, 2008, pp. 25–29.

[7] Carlo Menon, S Busolo, S Cocuzza, A Aboudan, A Bulgarelli, C Bettanini, M Marchesi, and F Angrilli, "Issues and solutions for testing free-flying robots," *Acta Astronautica*, vol. 60, no. 12, pp. 957–965, 2007.

[8] Wenfu Xu, Bin Liang, and Yangsheng Xu, "Survey of modeling, planning, and ground verification of space robotic systems," *Acta Astronautica*, vol. 68, no. 11–12, pp. 1629 – 1649, 2011.

[9] Yoji Umetani and Kazuya Yoshida, "Experimental study on two-dimensional free-flying robot satellite model," 1989.

[10] Marc A Ullman and Robert H Cannon Jr, *Experiments in autonomous navigation and control of a multi-manipulator, free-flying space robot*, Springer, 1993.

[11] Kazuya Yoshida, "Experimental study on the dynamics and control of a space robot with experimental free-floating robot satellite," *Advanced Robotics*, vol. 9, no. 6, pp. 583–602, 1994.

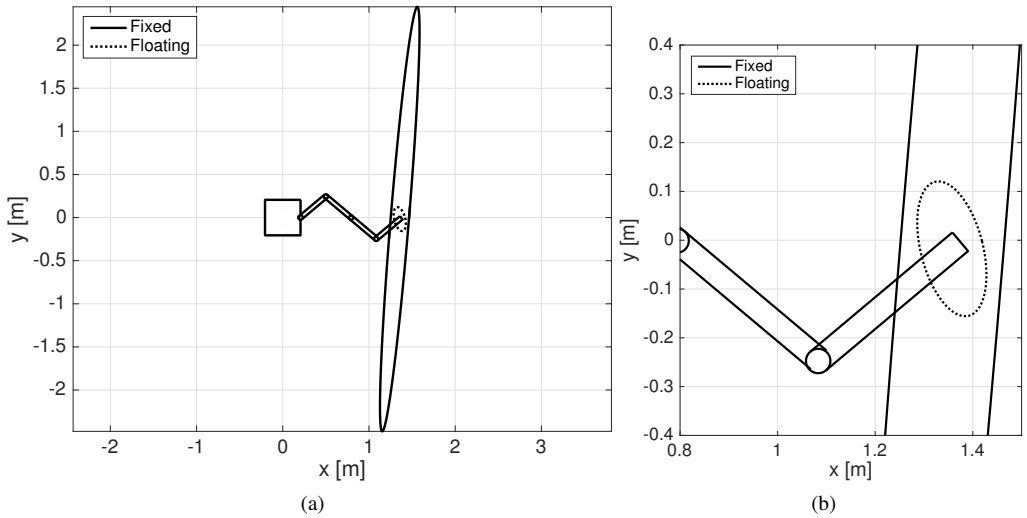

Fig. 8: Example of kinematic manipulability ellipsoid (with a detailed view of the floating-base manipullability in (b)).

[12] Z Pronk and P Th LM van Woerkom, "Flat-floor facilities im support of configurable space structures development," *Acta astronautica*, vol. 38, no. 4, pp. 277–288, 1996.

[13] C.R. Carignan and D.L. Akin, "The reaction stabilization of on-orbit robots," *Control Systems, IEEE*, vol. 20, no. 6, pp. 19–33, Dec 2000.

[14] Marcello Romano and Jason Hall, "A testbed for proximity navigation and control of spacecraft for on-orbit assembly and reconfiguration," in *Proceedings of the AIAA Space 2006 Conference and Exhibit*, 2006, pp. 1–11.

[15] Marcello Romano, David A. Friedman, and Tracy J. Shay, "Laboratory experimentation of autonomous spacecraft approach and docking to a collaborative target," *Journal of Spacecraft and Rockets*, vol. 44, no. 1, pp. 164–173, 2007.

[16] Jason S. Hall and Marcello Romano, "Novel robotic spacecraft simulator with mini-control moment gyroscopes and rotating thrusters," in *Advanced intelligent mechatronics, 2007 IEEE/ASME international conference on*. 2007, pp. 1–6, IEEE.

[17] Riccardo Bevilacqua, Jason S. Hall, James Horning, and Marcello Romano, "Ad hoc wireless networking and shared computation for autonomous multirobot systems," *Journal of Aerospace Computing, Information, and Communication*, vol. 6, no. 5, pp. 328–353, 2016/01/07 2009.

[18] Riccardo Bevilacqua, Andrew Caprari, Jason Hall, and Marcello Romano, "Laboratory experimentation of multiple spacecraft autonomous assembly," in *AIAA Guidance, Navigation and Control Conference and Exhibit*, 2009.

[19] Claudio Lugini and Marcello Romano, "A ballistic-pendulum test stand to characterize small cold-gas thruster nozzles," *Acta Astronautica*, vol. 64, no. 5, pp. 615–625, 2009.

[20] Fabio Curti, Marcello Romano, and Riccardo Bevilacqua, "Lyapunov-based thrusters' selection for spacecraft control: analysis and experimentation," *Journal of guidance, control, and dynamics*, vol. 33, no. 4, pp. 1143–1160, 2010.

[21] Jason S. Hall and Marcello Romano, *Laboratory experimentation of guidance and control of spacecraft during on-orbit proximity maneuvers*, INTECH Open Access Publisher, 2010.

[22] Marco Ciarcia, Alessio Grompone, and Marcello Romano, "A near-optimal guidance for cooperative docking maneuvers," *Acta Astronautica*, vol. 102, pp. 367–377, 2014.

[23] Richard Zappulla II, Hyeongjun Park, Josep Virgili Llop, and Marcello Romano, "Experiments on autonomous spacecraft rendezvous and docking using an adaptive artificial potential field approach," in *26th AAS/AIAA Space Flight Mechanics Meeting, Napa, CA. 14-18 February 2016. AAS 16-459*, 2016.

[24] K. Yoshida, K. Hashizume, and S. Abiko, "Zero reaction maneuver: flight validation with ets-vii space robot and extension to kinematically redundant arm," in *Robotics and Automation, 2001. Proceedings 2001 ICRA. IEEE International Conference on*, 2001, vol. 1, pp. 441–446 vol.1.

[25] Bruno Siciliano, Lorenzo Sciavicco, Luigi Villani, and Giuseppe Oriolo, *Robotics Modelling, Planning and Control*, Springer, 2009.

[26] Jacques Denavit and Richard Scheunemann Hartenberg, "A kinematic notation for lower-pair mechanisms based on matrices," *Journal of Applied Mechanics*, 1955.

[27] DCH Yang and TW Lee, "On the evaluation of manipulator workspace," *Journal of Mechanism, Transmission, Automation in Design*, vol. 105, pp. 70–77, 1983.

[28] Marco Ceccarelli, "A formulation for the workspace boundary of general n-revolute manipulators," *Mechanism and Machine Theory*, vol. 31, no. 5, pp. 637–646, 1996.

[29] JA Snyman, LJ Du Plessis, and Joseph Duffy, "An optimization approach to the determination of the boundaries of manipulator workspaces," *Journal of Mechanical Design*, vol. 122, no. 4, pp. 447–456, 2000.

[30] Karim Abdel-Malek, Harn-Jou Yeh, and Saib Othman, "Interior and exterior boundaries to the workspace of mechanical manipulators," *Robotics and Computer-Integrated Manufacturing*, vol. 16, no. 5, pp. 365 – 376, 2000.

[31] Jingzhou Yang, Karim Abdel-Malek, and Yunqing Zhang, "On the workspace boundary determination of serial manipulators with non-unilateral constraints," *Robotics and Computer-Integrated Manufacturing*, vol. 24, no. 1, pp. 60 – 76, 2008.

[32] Z. Vafa and S. Dubowsky, "On the dynamics of manipulators in space using the virtual manipulator approach," in *Robotics and Automation. Proceedings. 1987 IEEE International Conference on*, Mar 1987, vol. 4, pp. 579–585.

[33] Z. Vafa and S. Dubowsky, "The kinematics and dynamics of space manipulators: The virtual manipulator approach," *Int. J. Rob. Res.*, vol. 9, no. 4, pp. 3–21, Aug. 1990.